ELSEVIER

Catalysis Today 78 (2003) 519–527

CATALYSIS TODAY

www.elsevier.com/locate/cattod

Ultrafine niobate ceramic powders in the system $RE_xLi_{1-x}NbO_3$ (RE: La, Pr, Sm, Er) synthesized by polymerizable complex method

Monica Popa*, Masato Kakihana

Materials and Structures Laboratory, Tokyo Institute of Technology, Nagatsuta 4259, Midori-ku, Yokohama 226-8503, Japan

Abstract

Nanopowders of lithium niobate $LiNbO_3$ and rare earth (RE) substituted $LiNbO_3$–$RE_xLi_{1-x}NbO_3$, $x = 0.05$ (RE: La, Pr, Sm, Er) were synthesized using a simple technique as the polymerizable complex method, based on the Pechini-type reaction route. A mixed solution of citric acid and ethylene glycol with Li, Nb and RE ions was polymerized. The formation mechanism, the homogeneity and the structure of the obtained powders have been investigated by thermogravimetry, X-ray diffraction, Raman spectroscopy and scanning electron microscopy measurements. The X-ray diffraction analysis indicated the formation of perovskite-type oxides, which crystallize in rhombohedral system when the Li–Nb and Li–Nb–RE polymeric precursors were treated at temperatures as low as 500 °C for 2 h. No additional crystalline phases formed during calcinations, but shifting of the XRD peaks with the RE ion substitution for Li suggested that structural modification inside the LN is the same. The Raman spectroscopy data of $LiNbO_3$ substituted by RE were compared to the results of the unsubstituted system. The substitution dependence of frequency and damping in the $A_1(TO_2)$, $A_1(TO_3)$ and $E(TO_2)$ modes were employed to deduce the incorporation site of RE ions in $LiNbO_3$.

Keywords: $LiNbO_3$; Rare earth substitution; Polymerizable complex technique; Nanopowders; Raman spectroscopy; Fluorescence

1. Introduction

$LiNbO_3$ (referred to as LN) has drawn a lot of attention in the last years owing to its good intrinsic electro-optic behaviour and to its excellent nonlinear optical properties. LN is a key material for photonics, both for basic research and industrial applications [1]. Lithium niobate is ferroelectric at room temperature with large electro-optic and nonlinear coefficients, high optical damage threshold and birefringence, finding many applications because of its characteristic ferroelectric, piezoelectric and pyroelectric properties [2–4]. The studies of $LiNbO_3$ system and related materials are of great interest for the development of piezoelectric components for high temperature purposes, in integrated optoelectronics technology and waveguide lasers. Rare earth (RE) doped lithium niobate received considerable attention in recent years owing to laser applications. Doping with foreign ions of RE elements modifies the optical properties of the matrix and makes the system useful for applications as photorefractive devices, solid-state lasers, optical waveguides [5–7]. However, studies on the lattice location of the RE ions as well as on their symmetry and local environment are still lacking, in order to understand the microscopic processes induced by doping.

* Corresponding author. Tel.: +81-45-924-5310; fax: +81-45-924-5309.
E-mail address: pmonica1@rlem.titech.ac.jp (M. Popa).

0920-5861/02/$ – see front matter © 2002 Elsevier Science B.V. All rights reserved.
PII: S0920-5861(02)00345-0

The aim of the present research was to synthesize homogeneous nanopowders of RE substituted lithium niobate oxides with perovskite structures and to investigate the substitution effect on the lattice and the influence on their structure and properties. We used for the synthesis an aqueous solution environmentally friendly method. In the last years, a lot of interest was focused on the synthesis of multi-component oxide materials using solution techniques, as these methods offer many advantages compared to the conventional solid-state reaction [8]. Developments concerning new methods, especially solution techniques involving improvement of the synthesis conditions for obtaining pure phases in multi-component oxide materials have been applied with increasing interest. Potentially, these techniques allow a better mixing of the constituent elements and thus a better reactivity of the mixture to obtain pre-reaction products at lower temperatures, to lower the reaction temperature and to prepare fine and homogeneous powders [8,9]. The properties of the final materials obtained are strongly dependent on the preparation method. We propose the synthesis of $LiNbO_3$ using a simple Pechini-type, polymerizable complex (PC) method based on polyesterification between citric acid (CA) and ethylene glycol (EG) [8]. The use of polymeric precursors method leads to materials with rigorous stoichiometry control, higher reactivity when compared with powders synthesized by conventional route. Our method allows an easy control over the final stoichiometry, low processing temperature, without intermediate grinding and high surface areas of the resulting material.

In this research we report on the synthesis and characterization of $LiNbO_3$ and $RE_{0.05}Li_{0.95}NbO_3$ (RE: La, Pr, Sm, Er) powders by PC method, which has successfully been used to provide very homogeneous, single-phase powders at temperatures as low as 500 °C.

2. Experimental

2.1. Synthesis conditions

The synthesis procedure for powders of $LiNbO_3$, as well as for RE substituted $LiNbO_3$ is outlined in Fig. 1. A quantity of 0.5 mol of CA (Wako Pure Chemical Ind. Ltd., Osaka, Japan) was dissolved in 2 mol of water followed by the addition of 1 mmol of Li_2CO_3 and 2 mmol of Nb–ammonium complex (Kanto Chemicals Co. Inc., Tokyo, Japan). The RE compounds $La_2O_3{\cdot}3H_2O$, $Pr_2(CO_3)_3$, $Sm_2(CO_3)_3$, and $Er_2(CO_3)_3$, respectively, were added corresponding to 5% molar ratio substitution of Li in $LiNbO_3$. The resulted mixtures were magnetically stirred in order to obtain in the solution stable metal–CA complexes. Clear transparent solutions were thus obtained. After the complete dissolution at 60 °C for ∼2 h, 400 mmol of EG was added. The solutions were continuously stirred with a magnetic stirrer on a hot plate, and the temperature was slowly increased to ∼90 °C to remove the excess water and to accelerate the polyesterification reaction between CA and EG. The prolonged heating at 90 °C for 7 h produced a viscous and bubbly orange mass. No turbidity or precipitation were observed during the polymerization process. Heating of the polymeric resin at high temperatures, above 300 °C, causes a breakdown of the polymer. The resulting resin was treated in a mantle heater at 400–450 °C for over 3 h, in order to fully evaporate highly combustible species in the glassy mass and to burn down most of the organic constituents, i.e. to induce charring. The resulting material had the appearance of a dark brown sticky ash, which was slightly ground into a powder by a Teflon rod. The as-obtained powder is referred to as the “precursor” hereafter, and was heat-treated between 500 and 900 °C for 2 h.

2.2. Characterization

The synthesized materials were characterized by thermal analysis and thermogravimetry (DTA/TG) and the products obtained during different stages were characterized by X-ray diffractometry (XRD) and Raman spectroscopy. The microstructure of the materials was evaluated by scanning electron microscopy (SEM). The thermal behaviour of the citrate precursors was studied by thermogravimetry measurements up to 1000 °C in static air, with α-Al_2O_3 as a reference. A simultaneous DTA/TG apparatus (Type-2020, MAC Science, Japan) with a heating rate of 2°/min was used. Phase purities and crystal structure of the obtained materials were determined by XRD. The patterns were recorded using Cu Kα radiation ($\lambda = 1.5405$ Å) at a scanning rate of 2°/min in the (2θ) range from 15° to 75°; the evolution of significant peaks was studied

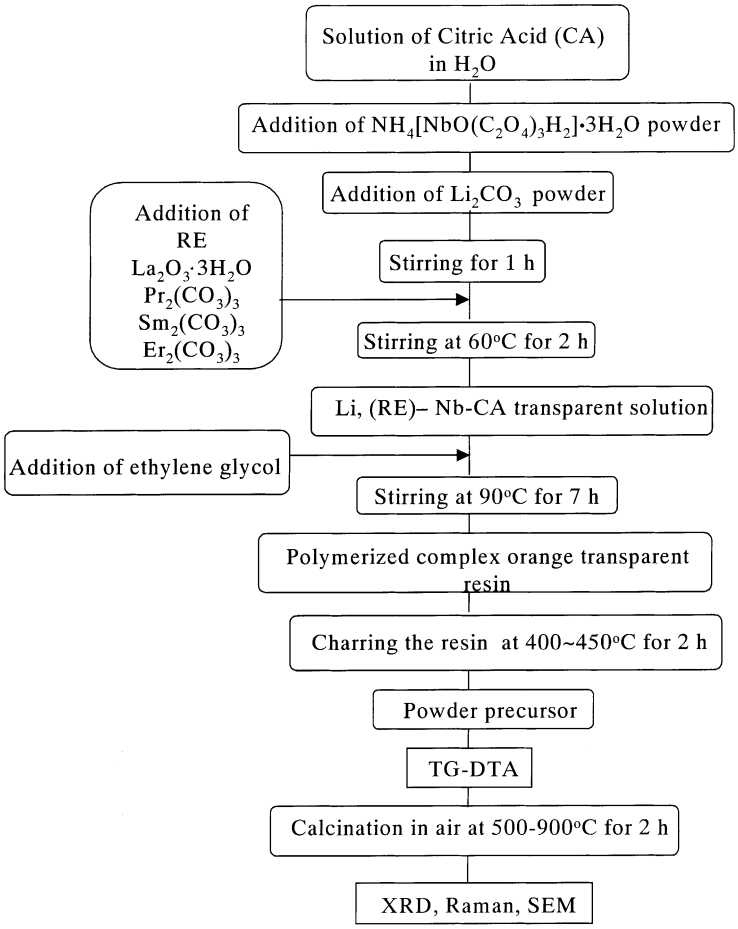

Fig. 1. Flow chart of the procedure used to prepare $LiNbO_3$ and $RE_{0.05}Li_{0.95}NbO_3$ perovskite oxide powders.

employing a scanning rate of 0.02° and counting time of 5 s per step. The SEM was performed in a Hitachi S-4500 scanning microscope for particle morphology and microstructure of the samples. The Raman spectra were performed at room temperature by using a triple spectrometer Jobin Yvon/Atago-Bussan T-6400 with a liquid nitrogen cooled CCD detector for 800 s, in micro-mode. The Ar^+ laser beam with the excitation $\lambda = 514.5$ nm was focused under 90× microscope objective and the laser spot size was between 1 and 2 μm. Raman spectra were recorded in 1000–100 cm^{-1} range. The spectral resolution was 1 cm^{-1}. The fluorescence of the samples was measured using a fluorescence spectrometer, type Hitachi F-4500 S.

3. Results and discussion

3.1. Thermal analysis events of $LiNbO_3$

Fig. 2 illustrates the TG/DTA/DTG curves of the powder precursor of $LiNbO_3$ obtained by the PC method, fired at 2 °C/min in the temperature range between 25 and 1000 °C. The TG curve shows a major weight loss step up to ~510 °C; no further weight loss was registered up to 1000 °C. The weight loss is related to the combustion of organic matrix. The clear plateau formed between 510 and 1000 °C on the TG curve indicates the formation of $LiNbO_3$ as decomposition product, as confirmed by X-ray analysis. On the DTA curve are observed two main exothermic

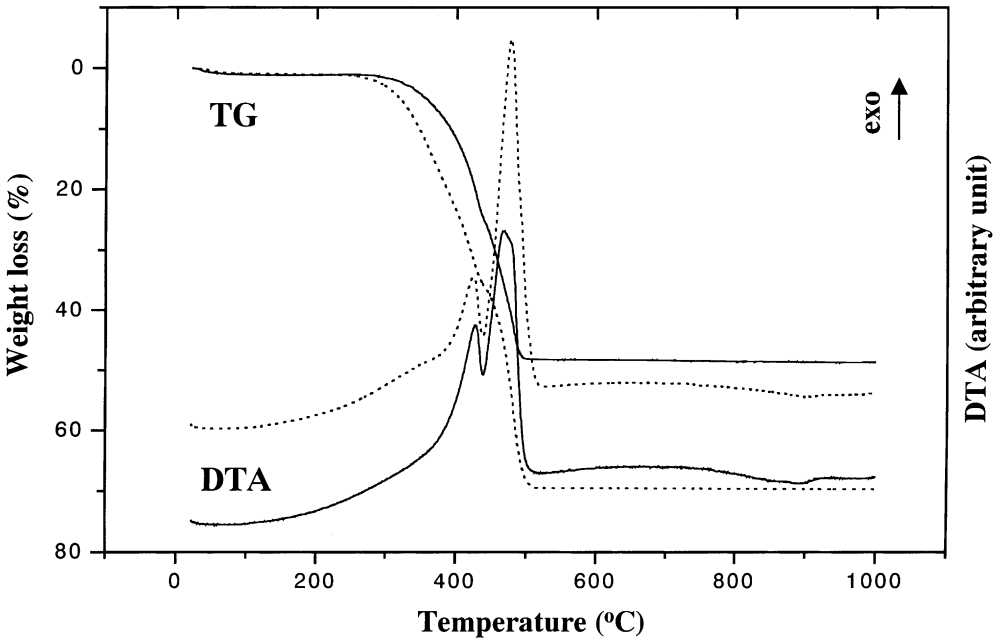

Fig. 2. The DTA/TG/DTG curves of the thermal decomposition of $LiNbO_3$ and Sm substituted $LiNbO_3$ perovskite oxide powders (represented with dotted lines) at a heating rate of 2°/min prepared by PC method.

effects with maxima at 430 and 468 °C, indicating that the thermal events can be associated with the burnout of organic species involved in the precursor powders (organic mass remained from CA and EG), of the residual carbon or due to direct crystallization of $LiNbO_3$ from the amorphous component. No further weight loss and no thermal effect was observed above 510 °C, indicating that no decomposition occurs above this temperature. Similar thermal behaviour was obtained for the RE substituted materials, therefore in Fig. 2, only the curves for Sm substituted $LiNbO_3$ are presented (with dotted lines).

3.2. Structure evolution analysis

The crystallization behaviour of solid precursors at different heat treatments was analysed by X-ray diffraction. Fig. 3 shows the XRD patterns of $LiNbO_3$ powder after calcination at 500, 700 and 900 °C for 2 h. The ash of the gels obtained after charring was amorphous (not shown in Fig. 3). All diffraction peaks were assigned as those from LN phase. It is of importance to mention that crystalline, single-phase per-

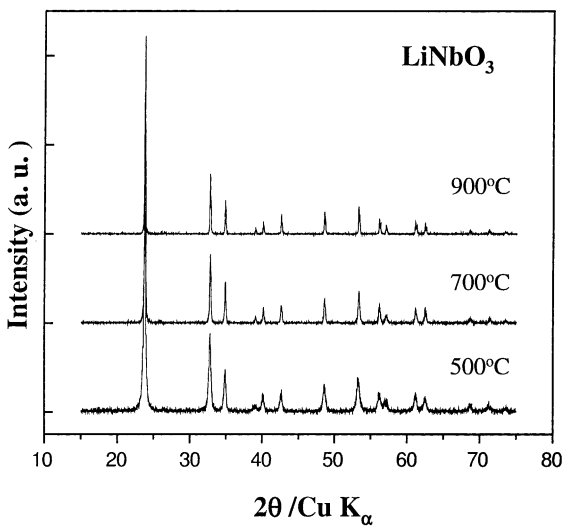

Fig. 3. X-ray diffraction patterns with Cu Kα radiation indexed with rhombohedral symmetry for $LiNbO_3$ perovskite oxide powders prepared by PC method, at different temperatures.

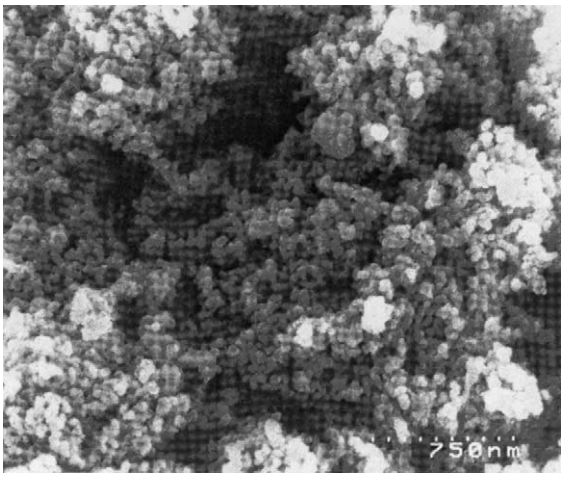

Fig. 4. SEM micrograph showing the particle size of $LiNbO_3$ perovskite powders prepared by PC method treated at 500 °C.

ovskite $LiNbO_3$ was obtained already at 500 °C from the decomposition of the complexes (JCPDS 20-631). Fine single-phase powders with particles in nanoscale range were obtained at temperatures as low as 500 °C. All powders presented similar structure with good homogeneity and uniform spherical grain size. Fig. 4 shows an example of microstructure of LN prepared by the PC method obtained at 500 °C. The mean particle size was in nanoscale range, between 40 and 60 nm. The SEM micrographs show a uniform grain size distribution, a fine powder size and homogeneous microstructure. Complete crystallization of $LiNbO_3$ takes place at 700 °C. The powder X-ray diffraction pattern revealed that sample belongs to a rhombohedral perovskite structure, with the average lattice parameters $a = 5.151$ Å and $c = 13.832$ Å. Even after calcinations at 900 °C the particle size of the powders was less than 100 nm, which is the usual lowest limit of most commercial powders [10]. Fig. 5 shows the X-ray diffraction patterns of RE substituted $LiNbO_3$. The XRD analysis showed that no additional crystalline phases formed during calcinations. There are subtle differences in the XRD patterns of the powders of RE substituted $LiNbO_3$. Fig. 6(a)–(c) exhibits the portion of XRD diagrams between 34.6° and 35.1°, 42.3° and 43° and 62.2° and 62.8° (2θ) of $Li_{0.95}RE_{0.05}NbO_3$ phases, showing the evolution of the peaks at (1 1 0), (2 0 2) and (3 0 0) with RE substitution and the shifting revealing the incorporation of the RE into the lattice.

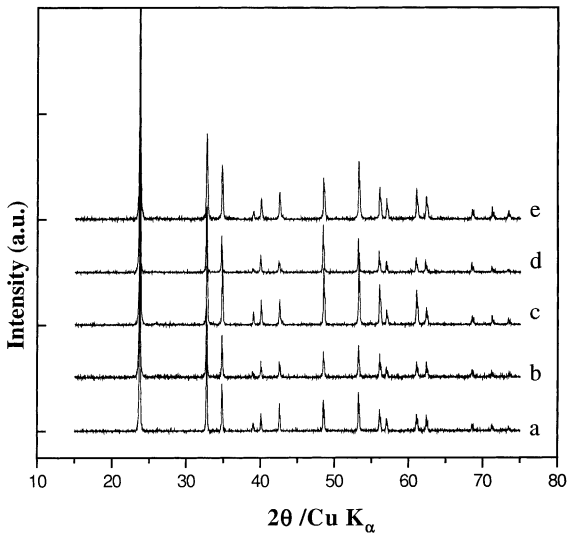

Fig. 5. X-ray diffraction patterns with Cu Kα radiation indexed with rhombohedral symmetry for $LiNbO_3$ (a) and $RE_{0.05}Li_{0.95}NbO_3$ (RE: La, Pr, Sm, Er) prepared by PC method (b: $Li_{0.95}La_{0.05}NbO_3$, c: $Li_{0.95}Pr_{0.05}NbO_3$, d: $Li_{0.95}Sm_{0.05}NbO_3$, e: $Li_{0.95}Er_{0.05}NbO_3$).

The reflections (1 1 0), (2 0 2) and (3 0 0) in the RE substituted LN rhombohedral structure broaden and shift with decreasing the ionic radii of the RE introduced into the LN matrix lattice. The shift of the peaks towards lower degrees increases with decreasing the ionic radius of the RE, except the case of Er^{3+} which has a slight shift compared to the pure LN peaks. From the structural point of view, XRD analysis has revealed no other phases that $LiNbO_3$, but shifting of the XRD peaks with the RE ion substitution for Li suggests that there is a structure modification inside the LN. Due to the relatively low concentration of these ions, X-ray diffraction alone cannot be used as a direct technique to determine the changes in the lattice. Therefore, the samples were analysed also by Raman spectroscopy.

3.2.1. Raman spectroscopy results

Raman spectroscopy is very sensitive to small modifications in the structure, by frequency shifts, damping of optical phonons or even by appearance of new lines in the Raman spectrum. At room temperature LN exhibits a ferroelectric rhombohedral structure belonging to the space group R3c (C_{3v}^6), with the primitive cell containing two formula units. Consequently, 18 vibration modes should be expected and are divided

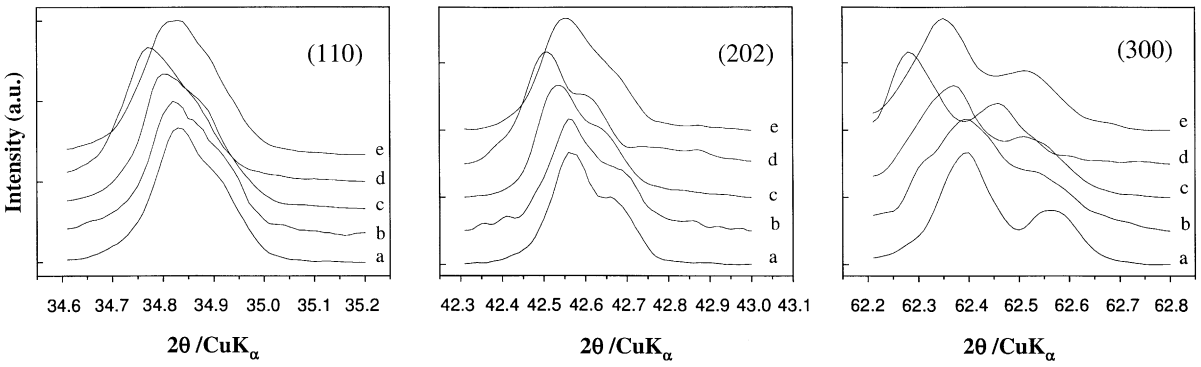

Fig. 6. (a–c) Portion of X-ray diffraction patterns of $LiNbO_3$ (a) and RE substituted $LiNbO_3$ powders $RE_{0.05}Li_{0.95}NbO_3$ (b: $Li_{0.95}La_{0.05}NbO_3$, c: $Li_{0.95}Pr_{0.05}NbO_3$, d: $Li_{0.95}Sm_{0.05}NbO_3$, e: $Li_{0.95}Er_{0.05}NbO_3$) showing the composition dependence of the lattice reflections (1 1 0), (2 0 2) and (3 0 0).

into $4A_1 + 9E + 5A_2$ in which A_2 phonons are Raman and IR inactive, while A_1 and E are both Raman and IR active. The assignments of the active frequencies in Raman and IR spectroscopies were proposed by different authors from polarization measurements [11–19]. In Fig. 7, the Raman spectra of RE substituted LN are compared to the spectrum of pure $LiNbO_3$. The assignments used in this work, in agreement with the results of Ridah et al. [16] and Repelin et al. [19] are given in Table 1. The mode frequencies in substituted powders are evaluated with respect of the values in unsubstituted samples. The spectra exhibit continuous changes on passing from pure LN to the RE substituted LN. Some peaks with clearly changes are observed,

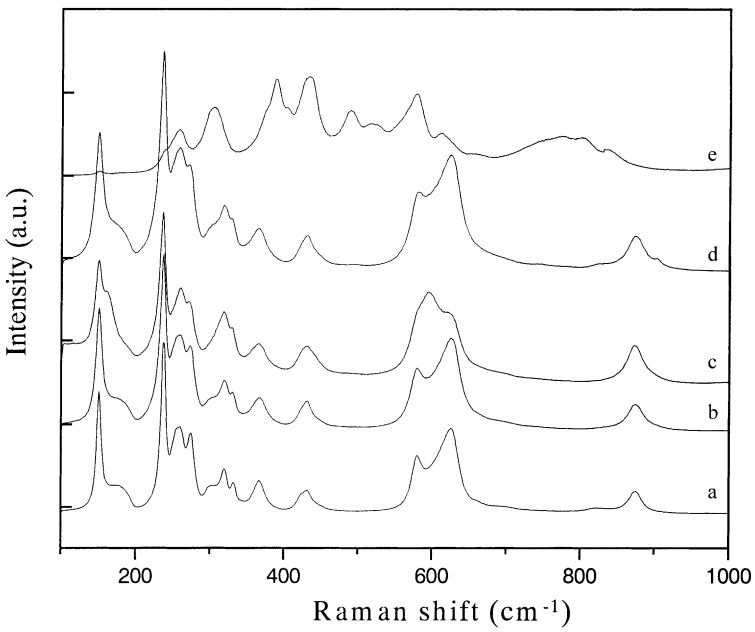

Fig. 7. Raman spectra of $LiNbO_3$ (a) and RE substituted $LiNbO_3$ powders $RE_{0.05}Li_{0.95}NbO_3$ (b: $Li_{0.95}La_{0.05}NbO_3$, c: $Li_{0.95}Pr_{0.05}NbO_3$, d: $Li_{0.95}Sm_{0.05}NbO_3$, e: $Li_{0.95}Er_{0.05}NbO_3$) $LiNbO_3$ powders obtained at 900 °C.

Table 1
Raman mode assignments (frequencies in cm^{-1}) for the powders of LN obtained by PC method

Mode assignments for $LiNbO_3$					
Our work		Ridah et al. [16]		Repelin et al. [19]	
A_1	E	A_1	E	A_1	E
625		633		630	
	610		610		610
	579		582		581
	431		431		431
	367		371		388
332		334		364	
	319		325		333
274		276		294	
	259		265		–
255		255		257	
	237		238		238
	178		180		180
	151		155		155

especially with decreasing the RE ionic radii. The Raman spectra evolution with the RE substituent shows that frequencies in the 100–370 and 570–630 cm^{-1} are influenced by RE presence. The determination of the site occupied by trivalent RE ions in LN is quite complicated because of the fact that four cationic lattice sites can be in principle occupied by RE^{3+} ions: three octahedral sites (Li^+, Nb^{5+} and a free/vacant octahedron) and an interstitial tetrahedral site. It is important to mention that according to the results that have been obtained for RE^{3+} ions lattice position in LN, is generally concluded that trivalent RE ions enter Li^+ octahedral sites in the host LN. For single doped $LiNbO_3$, the foreign ions are located near the Li lattice. Similar results have been obtained for other RE^{3+}: Pr, Eu, Ho, Yb. As a general behaviour, it is concluded that trivalent rare ions enter Li^+ octahedral sites in the LN host crystal, as these ions are heavier than Nb^{5+} which is the heaviest ion in the host LN [20,21]. First, we analysed the effect of substitution on mode frequencies and we noticed that the spectra of the substituted LN with RE differ from that of the LN. It can be observed that the substitution of Li by RE determines a broadening and a merging of the bands in the mentioned ranges, going from La to Er, from the RE with bigger radius to the RE with the smaller radius. The frequency of the band at 178 cm^{-1} ($E(TO_2)$) in unsubstituted LN as well as the bands at 274 cm^{-1} ($A_1(TO_2)$), 332 cm^{-1} ($A_1(TO_3)$) and 367 cm^{-1} ($E(TO_6)$) registrate an increase in the phonon damping in the samples substituted by RE, while the bands $A_1(TO_1)$ and $E(TO_1)$ exhibit the same behaviour versus substitution, in agreement with previous observations in similar systems [22]; the bands $A_1(TO_1)$, which represents the vibration of Nb in antiphase with the oxygen plane along the trigonal axis and $E(TO_1)$, which represents the deformation of the BO_6 (NbO_6) in the (x, y) plane remain almost unaffected by substitution. In our case, $A_1(TO_2)$ and $A_1(TO_3)$ are the modes which are most affected by the substitution, as the bands are shifted from their fundamental frequency in LN, from 274 to 270 cm^{-1} and from 332 to 328 cm^{-1}; the lowest band can be seen in the case of Pr substitution, where the mode was observed at 270 cm^{-1}. Since the most significant change in frequency exhibits the mode $A_1(TO_2)$ which exhibits a substantial amount of Li movement and $A_1(TO_3)$ which is the rotation of whole oxygen octahedra along the trigonal axis (motion of oxygen anions only), RE ions are on the A sites, is in agreement with the results published by Mouras et al. [22] and Zhang et al. [23]. The decrease in frequency of $E(TO_2)$ from 178 cm^{-1} in LN to 176 cm^{-1} in Sm substituted LN, shows that the RE occupy also the B lattice sites, especially in the case of Pr. The Raman spectrum obtained for Er substituted LN is different from the other spectra. We used the 514.5 nm excitation line to record both the lattice vibration spectrum and the fluorescence spectrum in the same wavenumber range for LN substituted with Er. There is an overlap between the lattice vibration and the fluorescence spectra, a partial mixing of the two spectra occurs. This requires 488 nm line as preferred excitation wavelength in accordance with Zhang et al. [24]; as the modes reported here were overlapped, a study using various excitation wavelengths especially for Er^{3+} case is very informative. Such kind of work is ongoing. Fig. 8 shows a total site selective contour plot of Er^{3+} substituted $LiNbO_3$ in the excitation wavelength from 200 to 600 nm and emission wavelength range 500–600 nm. A careful inspection of the spectrum reveals the presence of fluorescence centres. In the "spectroscopy map" obtained from tri-dimensional spectra (excitation, emission, intensity) recorded at room temperature, intensity appears as contours (constant), while the excitation and emission wavelengths are the x, y axes. In agreement with other reported

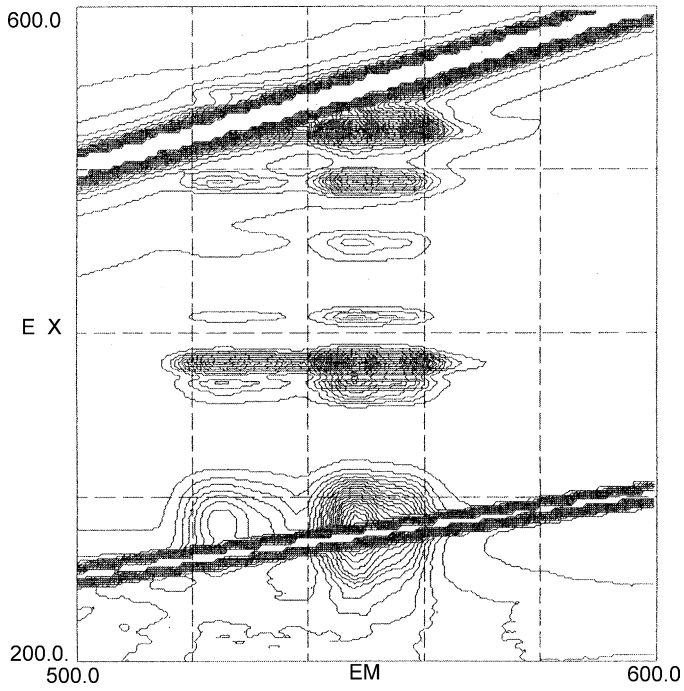

Fig. 8. Fluorescence map of the Er substituted $LiNbO_3$.

results [25,26], from the map can be observed the centres in the emission spectra for each particular excitation wavelength. More studies are needed in order to determine the influence of RE on the properties and structure of LN.

4. Conclusions

$RE_{0.05}Li_{0.95}NbO_3$ (RE: La, Pr, Sm, Er) powders were obtained at temperatures as low as 500 °C without the presence of any secondary phases, using a simple environmentally friendly technique: PC method. The method makes possible the synthesis of very fine, homogeneous powders with particles in nanoscale range. From the structural point of view, XRD analysis for the RE substituted LN, has revealed no other phases that $LiNbO_3$, but shifting of the XRD peaks with the RE ion substitution for Li suggests that structural modification inside the LN is the same. The Raman spectroscopy results allowed us to assign and describe the vibrational modes in LN as well as to analyse the evolution of the modes in RE substituted LN. The $A_1(TO_2)$, $A_1(TO_3)$ and $E(TO_2)$ were the modes which were most affected by the substitution, as the bands were shifted from their fundamental frequency in LN. Based on Raman spectroscopy results we can conclude that RE^{3+} ions lie in Li^+ sites. The fluorescence centres in the emission spectra of Er substituted LN for different excitation wavelengths were shown. This basic research should be useful to study and understand the substitution effect of RE ions for Li, in powders of LN.

References

[1] F. Caccavale, A. Morbiato, N. Natali, C. Sada, F. Segato, J. Appl. Phys. 87 (2000) 1007.
[2] C.D.E. Lakeman, D.A. Payne, Mater. Chem. Phys. 38 (1994) 305.
[3] S. Lanfredi, S.F. Dominguez, A.C.M. Rodrigues, J. Mater. Chem. 5 (1995) 1957.
[4] S. Lanfredi, A.C.M. Rodrigues, J. Appl. Phys. 86 (1999) 2215.
[5] E. Kratzig, O.F. Schirmer, Photorefractive Materials and Their Applications I, Springer Topics in Applied Physics 61, Springer, Berlin, 1988.

[6] L.F. Johnson, A.A. Ballman, J. Appl. Phys. 40 (1969) 297.
[7] M.N. Armenise, C. Canali, M. de Sario, E. Zanoni, Mater. Chem. Phys. 9 (1983) 267.
[8] M. Kakihana, J. Sol.-Gel. Sci. Technol. 6 (1996) 5.
[9] M. Kakihana, M. Yoshimura, Bull. Chem. Soc. Jpn. 72 (1999) 1427.
[10] Y. Jorand, M. Taha, J.M. Missiaen, L. Montanaro, J. Eur. Ceram. Soc. 15 (1995) 469.
[11] Y.-C. Ge, L.-X. Li, C.-Z. Zhao, Spectr. Lett. 30 (1997) 567.
[12] C. Raptis, Phys. Rev. B 38 (1988) 10007.
[13] A.F. Penna, R.P. Andrade, S.P.S. Porto, Phys. Rev. B 13 (1976) 4907.
[14] D. Johnston Jr., I.P. Kaminov, Phys. Rev. 168 (1968) 1045.
[15] N.V. Sidorov, M.N. Palatnikov, Yu A Serebryakov, E.L. Lebedeva, V.T. Kalinnikov, Inorg. Mater. 33 (1997) 419.
[16] A. Ridah, P. Bourson, M.D. Fontana, G. Malovichko, J. Phys. Condens. Matter. 9 (1997) 9687.
[17] R.F. Schaufele, J. Weber, Phys. Rev. 152 (1966) 705.
[18] A.S. Barker, R. Loudon, Phys. Rev. 158 (1967) 433.
[19] Y. Repelin, E. Husson, F. Bennani, C. Proust, J. Phys. Chem. Solids 60 (1999) 819.
[20] A. Lorenzo, H. Loro, J.E. Munoz, Santiuste, M.C. Terille, G. Boulon, L.E. Bansa, J. Garcia Sole, Opt. Mater. 8 (1997) 55.
[21] A. Lorenzo, H. Jaffrezic, B. Roux, G. Boulon, J. Garcia Sole, Appl. Phys. Lett. 67 (25) (1995) 3735.
[22] R. Mouras, P. Bourson, M.D. Fontana, G. Boulon, Optics Commun. 197 (2001) 439.
[23] D. Zhang, X. Chen, Y. Wang, D. Zhu, B. Wu, G. Lan, J. Phys. Chem. Solids 63 (2002) 345.
[24] D. Zhang, X. Chen, Y. Jin, X. Cao, D. Zhu, Y. Wang, G. Ding, Y. Cui, C. Chen, Z. Wu, G. Lan, Appl. Phys. A 72 (2001) 95.
[25] D.M. Gill, J.C. Wright, L. McCaughan, Appl. Phys. Lett. 64 (19) (1994) 2483.
[26] D.M. Gill, L. McCaughan, J.C. Wright, Phys. Rev. B 53 (1996) 2334.